Active materials embedded in photonic crystals and coupled to electromagnetic radiation

Peter Bermel, Elefterios Lidorikis, Yoel Fink, and John D. Joannopoulos
Center for Materials Science and Engineering, Massachusetts Institute of Technology, Cambridge, Massachusetts 02139, USA
(Received 8 November 2005; revised manuscript received 8 February 2006; published 25 April 2006)

A calculational scheme is presented to model the interaction of light with active dielectric media, represented by four-level atomic materials, surrounded by photonic crystals. Optically pumped lasing is studied in three model systems: a Fabry-Perot cavity, a line of defects in a two-dimensional square lattice of rods, and a cylindrical photonic crystal. Field profiles and conversion efficiencies are calculated for these systems. It is shown that high conversion efficiency can be achieved for large regions of active material in the cavity, as well as for a single fluorescent atom in a hollow-core cylindrical photonic crystal, suggesting designs for ultralow-threshold lasers and ultrasensitive biological sensors.

DOI: 10.1103/PhysRevB.73.165125 PACS number(s): 42.70.Qs, 42.79.Gn

I. INTRODUCTION

The interaction of light with active materials can give rise to a rich variety of physical phenomena, such as material dispersion,[1] plasmons,[2] polaritons,[3] and spontaneous and stimulated emission.[4] These phenomena are the basis of a wide variety of technologically important devices, such as fiber optics,[1] lasers,[1] and photovoltaic cells.[5] They can all be understood with the semiclassical physical model of harmonic oscillators coupled to electromagnetic fields. However, while simple analytical expressions can be written down, accurate solutions for realistic systems require a numerical solution. The most detailed model of four-level atomic systems tracks fields and occupation numbers at each point of the computational cell, taking into account energy exchange between atoms and fields, electronic pumping, and nonradiative decays.[4]

This paper aims to apply a detailed computational model to the problem of lasing. The basics of optical lasing have been understood theoretically since 1958: an atomic system is put in a resonant cavity and excited to a population-inverted state, which then leads to stimulated emission of coherent photons.[6] Quantities such as lasing threshold and efficiency can be calculated approximately using simple analytical expressions. However, exact calculations of efficiency or nonequilibrium dynamics are still considered to be challenging. Many groups in the past have employed approximations to simplify their calculations—e.g., using a current source,[7] a fixed conductivity,[8] or randomly distributed dipole sources.[9,10] In an attempt to achieve more realistic simulations, it has been shown that two-level Maxwell-Bloch equations can be solved using iterative predictor-corrector finite-difference time-domain (FDTD) methods to demonstrate saturation and self-induced transparency.[11,12] This approach has also been applied to objects with one-dimensional (1D) periodicity which may act as couplers, modulators, and switches[13] and has been extended to three-level atoms using pseudospin equations.[14] In a different area, researchers have now begun to study random laser systems by directly simulating semiclassical atoms interacting with electromagnetic fields. This work began with simulations of four-level atoms in 1D that demonstrated lasing is indeed possible in random systems.[15–17] More recent work demonstrates that random arrangements of 2D rods can also give rise to random lasing.[18,19] A much more thorough review of recent work in random lasing, both theory and experiment, can be found in Ref. 20. Along slightly different lines, using two-level Maxwell-Bloch equations, it has been shown that electrically pumped atoms inside a 2D high-index cavity can give rise to lasing.[21] On a related note, Ref. 22 has developed a simulation scheme for four-level two-electron atomic systems which demonstrate a different lasing threshold than observed for the semiclassical lasing equations in Ref. 4.

Nonetheless, all of these calculations have been done in 1D or 2D systems and, to the best of our knowledge, have not been applied to photonic crystals with periodicity in more than one direction. In this paper, this type of approach is extended to 3D systems and results are obtained for photonic crystal systems of each dimensionality. This paper begins with a discussion of the computational approach and verification of the code with an analytically soluble problem. This code is then applied to a Fabry-Perot cavity with atomic material in the defect region. Next, a 2D problem is considered, a photonic crystal consisting of a square lattice of rods with a line of defects. Finally, a 3D problem is considered, a cylindrical photonic crystal with a region of atomic material.

II. THEORY

The theoretical approach is as follows. The electric fields and occupation numbers N_j for a four-level atomic system ($j=0,1,2,3$) are modeled semiclassically, with all quantities being tracked at every point in the computational cell (following Ref. 4). Maxwell's equations are given by $\nabla\times\mathbf{E}=-(1/c)\partial\mathbf{H}/\partial t$ and $\nabla\times\mathbf{H}=4\pi\mathbf{j}/c+(1/c)\partial\mathbf{D}/\partial t$ with the constitutive relation $\mathbf{D}=\epsilon_p\mathbf{E}+4\pi\Sigma_{i=1,2}\mathbf{P}_i$, where ϵ_p is the dielectric function of the passive medium (i.e., in the absence of active materials) and where $\mathbf{P}_i$ is the ith electronic polarization density of the active material. This polarization density behaves as a harmonic oscillator driven by the product of the external field and the population inversion and is given by

$$\frac{d^2\mathbf{P}_i}{dt^2}+\Gamma_i\frac{d\mathbf{P}_i}{dt}+\omega_i^2\mathbf{P}_i=\sigma_i\Delta N_i\mathbf{E}, \tag{1}$$

where Γ_i is the nonradiative decay width for $\mathbf{P}_i$, σ_i is the coupling strength of $\mathbf{P}_i$ to the external electric field, and $\Delta N_1=N_1-N_2$ and $\Delta N_2=N_0-N_3$ are the population inversions

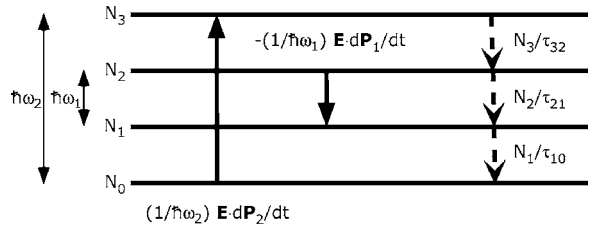

FIG. 1. Relationships between energy levels in the four-level atomic system used in this paper. Straight lines correspond to radiative transitions; dashed lines correspond to nonradiative transitions.

that drive the polarizations. The occupation numbers vary according to the following equations:

$$\frac{dN_3}{dt} = \frac{1}{\hbar\omega_2}\mathbf{E}\cdot\frac{d\mathbf{P}_2}{dt} - \frac{N_3}{\tau_{32}}, \tag{2}$$

$$\frac{dN_2}{dt} = \frac{1}{\hbar\omega_1}\mathbf{E}\cdot\frac{d\mathbf{P}_1}{dt} + \frac{N_3}{\tau_{32}} - \frac{N_2}{\tau_{21}}, \tag{3}$$

$$\frac{dN_1}{dt} = -\frac{1}{\hbar\omega_1}\mathbf{E}\cdot\frac{d\mathbf{P}_1}{dt} + \frac{N_2}{\tau_{21}} - \frac{N_1}{\tau_{10}}, \tag{4}$$

$$\frac{dN_0}{dt} = -\frac{1}{\hbar\omega_2}\mathbf{E}\cdot\frac{d\mathbf{P}_2}{dt} + \frac{N_1}{\tau_{10}}. \tag{5}$$

Terms such as $\frac{1}{\hbar\omega_1}\mathbf{E}\cdot\frac{d\mathbf{P}_1}{dt}$ represent the conversion between atomic potential energy and field energy at a certain rate. A population inversion will drive the polarization field $\pi/2$ radians out of phase with the external electric field, which converts atomic potential energy into field energy—the semiclassical version of stimulated emission. Other terms such as $\frac{N_2}{\tau_{21}}$ are nonradiative decays between adjacent levels; this energy is considered to be lost. The interactions between the energy levels are illustrated in Fig. 1. Decay rates play an important role in determining the efficiency of any optical pumping process. In this paper, efficiency is defined as the ratio of the number of optical transitions at the emitting frequency to the number of optical transitions at the absorbing frequency—i.e.,

$$\eta = \frac{\frac{1}{\hbar\omega_1}\int_0^\infty dt\left[\mathbf{E}\cdot\frac{\partial\mathbf{P}_1}{\partial t}\right]}{\frac{1}{\hbar\omega_2}\int_0^\infty dt\left[\mathbf{E}\cdot\frac{\partial\mathbf{P}_2}{\partial t}\right]}. \tag{6}$$

This quantity effectively measures the competition between radiative and nonradiative decay processes and approaches 1 in the limit where the stimulated emission rate is much greater than the nonradiative decay rate. As a result, η will generally go up with incoming beam power, as well as with an increase in the lifetime of the metastable state τ_{21}. This relationship, which includes lasing threshold-type behavior, is quantified in Sec. III B, below.

In order to solve the behavior of active materials in electromagnetic fields numerically, the FDTD technique[23] is utilized, using an approach similar to the one outlined in Ref. 16. Both time and space are discretized into steps small compared to the characteristic periods and wavelengths of the problem, and at each point the electric, magnetic, and polarization fields are initialized to zero, while the atomic fields are initialized to their ground states. The following steps are taken to evolve the fields in time. First, the polarizations are integrated through one time step using Eq. (1) [tracking the two values at each point needed for any second-order ordinary differential equation (ODE)]. Next, the electric fields are integrated according to the Maxwell-Ampère law (which includes subtracting the polarizations from the electric field). Finally, the atomic occupations N_j are integrated according to Eqs. (2)–(5), and the magnetic fields are integrated according to Faraday's law (these last two steps can be done in either order). The cycle is repeated for each time step until all electric, magnetic, and polarization fields have decayed to negligible magnitudes.

In this work, stimulated emission at frequency ω_1 is desired, which requires a population inversion between the two intermediate levels separated by energy $\hbar\omega_1$. Photonic crystals can enhance such stimulated emission when the absorption and emission frequencies and widths are chosen so that an excitation frequency above the photonic band gap drives atomic material present in a defect region to emit into a resonant mode inside the band gap. For generality, we choose to model our active material as an adjustable four-level atomic system. The field amplitudes, coupling strengths, and decay rates are chosen to ensure that a substantial fraction of atoms absorb fields of frequency ω_2 and then produce a population inversion, thereby amplifying fields of frequency ω_1. The decay times τ_{32} and τ_{10} are chosen to be quite small—e.g., 200 time steps—just large enough to achieve a smooth decay curve for the upper level. The decay time τ_{21} is chosen to be several orders of magnitude larger than the other decay times τ_{32} and τ_{10} to simulate a metastable state. Clearly, the conversion between the excitation and emission frequencies will be most efficient for the largest values of τ_{21}. Furthermore, the decay widths should be chosen so that the width associated with the higher-frequency absorbing transition, Γ_2, is relatively large to maximize absorption and so that the width associated with the lower-frequency emission transition, Γ_1, is relatively small, in order to match the quality factor of the resonant mode in the photonic crystal. The choice of coupling strengths σ_i and field amplitudes are closely related. The appropriate values can be calculated through the following approach. First, note that in a steady state, $\mathbf{P}_i(\omega) = \frac{\sigma_i \Delta N_i}{\omega_i^2 - \omega^2 - i\omega\Gamma_i}\mathbf{E}(\omega)$. As a result, the on-resonance response to a continuous-wave (cw) source in the time domain will be $\mathbf{P}_i(t) = \frac{\sigma_i \Delta N_i}{-i\omega_i\Gamma_i}\mathbf{E}(t)G(t)$, where $G(t)$ is a turn-on function that rises from 0 to 1 as one approaches the steady state, with the approximation of constant ΔN_i. The total radiative population transfer from the ground state to the metastable excited state can then be estimated from Eq. (2) to be $N_2 \approx \frac{\sigma_2 \Delta N_2}{\hbar\omega_2\Gamma_2}\int dt[\mathbf{E}(t)]^2 G(t)$ for a cw source (assuming the population transferred to level 3 quickly drops down to level 2 and then stays there). For a pulsed source with a finite spectral width, but a duration greater than the turn-on time (which should be a few periods), we can simplify our expres-

sion by setting $G(t)=1$ and then transform to the frequency domain using Parseval's theorem. We then keep all frequencies close to the resonant frequency (within $\pm\Gamma_2/2$) and discard the rest, giving us

$$N_2 \approx \frac{\sigma_2 \Delta N_2}{\hbar \omega_2 \Gamma_2} \int_{\omega_2-\Gamma_2/2}^{\omega_2+\Gamma_2/2} |E(\omega)|^2 d\omega \equiv \frac{\sigma_2 \Delta N_2}{\hbar \omega_2 \Gamma_2} I_2, \qquad (7)$$

where I_2 is an intensity integral whose numerical value is given later for each simulation with a pulsed source. Equation (7) can readily be used to calculate the field amplitudes needed to achieve a given level of population inversion in the limit that ΔN_2 is approximately constant. Now, we seek to calculate the criteria for lasing. We assume a resonant mode of a high-Q cavity with frequency ω_1 is initially excited at time 0 with a small amplitude. The associated polarization field is expected to have the form $P_1=P_0 e^{-i\omega_1 t} e^{\alpha t}$, where α is a growth rate that is assumed to be small relative to the frequency ω. Then we can substitute into Eq. (1) to find that, to the lowest order in α, $2\alpha+\Gamma_e = (\sigma_1/\omega_1)|\Delta N_1(0) E/P_1|$, where the $\Delta N_1(0)$ is the initial population inversion and $\Gamma_e=\Gamma_1+2\tau_{21}^{-1}$ is the total loss rate for a pulsed excitation, while $\Delta N_1(0) \rightarrow \Delta N_1$ and $\Gamma_e=\Gamma_1$ for a continuous-wave pulse. In order to achieve exponential growth of the mode, it must then be the case that $(\sigma_1/\omega_1)|\Delta N_1(0) E/P_1| > \Gamma_e$. If the system reaches the regime where the electric field is driven by the polarization field—i.e., $E=-4\pi P_1$—then we obtain the condition for sustainable growth, $|\Delta N_1(0)| > \omega_1 \Gamma_e / 4\pi\sigma_1$.

III. SIMULATIONS

A. Two-level atomic system

The first simulation checks the agreement of the code with an analytical model for the upper-level occupation. It can be shown that for a two-level atomic system stimulated by an external plane-wave cw source with a finite rate of nonradiative decay, the steady-state upper-level occupation N_2 should behave as

$$N_2 = \frac{1}{2}\left[\frac{1}{1+\left(\frac{\hbar\omega\Gamma}{\tau\sigma}\right)\frac{1}{|E|^2}}\right], \qquad (8)$$

where $|E|$ is the amplitude of the external plane-wave cw source, ω is the frequency of the source and the atomic resonance, Γ is the width of the atomic resonance, τ is the rate of nonradiative decay, and σ is the coupling strength.

A series of simulations are then performed in which a slab of the two-level atomic material is subjected to a cw source of frequency $\omega=0.25(2\pi c/a)$ (where a is the period of a photonic crystal) and allowed to equilibrate. This is done for two cases: an atomic slab surrounded by vacuum and an atomic slab enclosed in a Fabry-Perot cavity with three quarter-wave-thick layers of polystyrene ($n=1.6$) and indium phosphide ($n=2.97$). The cavity is designed to exhibit a resonance at the cw source frequency. The steady-state upper-level occupation number is then measured for a series of different values of the incident field amplitude. As can be seen in Fig. 2, the simulation nicely reproduces the analytical prediction for both cases. There are two regimes for both curves in this figure. For low field amplitudes $\left(|E| \ll \sqrt{\frac{\hbar\omega\Gamma}{\tau\sigma}}\right)$, the occupation grows quadratically with field amplitude [i.e., $N_2 \approx \left(\frac{\tau\sigma}{2\hbar\omega\Gamma}\right)|E|^2$], which corresponds to the physical picture that the atoms absorb a fixed fraction of the incident light, as would be seen in a nonatomic material with a constant conductivity. On the other hand, for large field amplitudes $\left(|E| \gg \sqrt{\frac{\hbar\omega\Gamma}{\tau\sigma}}\right)$, the occupation saturates to the maximum value of one-half (corresponding to equal occupations of the upper and lower levels). In this simulation, we choose $\hbar\omega\Gamma/\tau\sigma=0.8$ and find that the curve of Fig. 2 precisely follows the analytical prediction of Eq. (8). The saturation occurs significantly earlier for the Fabry-Perot cavity because of the substantial resonant enhancement of electric field magnitudes, which also enhances polarization field magnitudes and the energy transfer rate. This phenomenon can also be viewed as an effective increase in the coupling strength of the polarization to the external field. For this calculation, a cavity with $Q=38$ shows an effective coupling enhancement factor of 24. Higher-quality factors should lead to even greater enhancements of the effective coupling.

B. Four-level atomic system

In this section, we consider a series of simulations in which a slab of four-level atomic material surrounded by vacuum is subjected to a cw source and allowed to equilibrate. The intensity of the cw source is varied, and then the power absorbed at the cw source frequency ω_2 is measured and compared to the power emitted at the target emission frequency ω_1. For the absorption frequency, we use $\omega_2=0.4(2\pi c/a)$, $\sigma_2=0.001(2\pi c/a)^2$, and $\Gamma_2=0.01(2\pi c/a)$; for the emission frequency, we use $\omega_1=0.2(2\pi c/a)$, $\sigma_1=0.02(2\pi c/a)^2$, and $\Gamma_1=0.001$. For the decay parameters, we use $\tau_{32}=2.5(a/c)$, $\tau_{21}=62.5(a/c)$, and $\tau_{10}=2.5(a/c)$. The results for power emitted versus power absorbed are plotted in Fig. 3. According to Sec. II, we expect the threshold to be crossed when $|\Delta N_1| > (\omega_1\Gamma_1/\sigma_1)|P_1/E| \approx 0.0132/4\pi$, since $|P_1/E|=1.32/4\pi$ in our calculation. For the first point above threshold, where $P_{in}=0.003\,04$ and $P_{out}=0.000\,149$, we find $\Delta N_1=0.0157/4\pi$, which puts us just above the critical value required for lasing. This demonstrates that lasing can occur in this system and that we are able to accurately predict the onset of lasing behavior. However, we are obliged to include the caveat that in a cavity, the rate of spontaneous emission will be modified in a way that is not included in the framework of our calculations. Therefore, while we observe that lasing occurs in the rest of the systems in the numerical part of this paper for sufficient power levels, we note that the threshold could be slightly higher than we calculate with this calculational scheme (but still substantially lower than in vacuum). In any case, despite this limitation, we are confident that lasing should still occur for sufficient power, and therefore the results in the subsequent sections should be

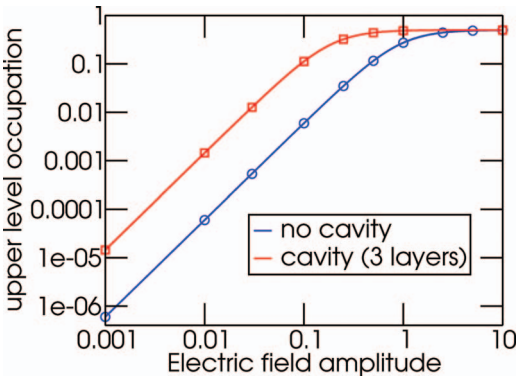

FIG. 2. (Color) Fractional occupation of the upper level of a two-level atomic system as a function of field amplitude, with and without a cavity. The symbols are simulation data, and the smooth curve represents a fit to Eq. (8). Two regimes are seen: at low field amplitudes, occupation goes up linearly with field intensity, and at high field amplitudes, occupation saturates at one-half. Saturation occurs more quickly with a cavity due to the enhancement of stimulated emission.

considered essentially valid. Also, note that the efficiency η associated with these processes will be given by the ratio of actual P_{out} to the theoretical limit $(\omega_1/\omega_2)P_{in}$ and will approach unity for values well above threshold.

C. Four-level atomic system in a Fabry-Perot cavity

Having verified that the code behaves properly, let us now consider a slightly more complex 1D system, as illustrated in Figs. 4 and 5. It consists of a Fabry-Perot étalon, made of four and a half bilayers of the high contrast dielectric materials tellurium ($n=4.8$) and polystyrene ($n=1.6$), enclosing a cavity of length $2.5a$ containing four-level atomic material described by Eqs. (2)–(5). A Gaussian plane-wave source with central frequency $\omega=0.4(2\pi c/a)$ is used to optically pump atoms contained inside the defect cavity that absorb at the same frequency $\omega=0.4(2\pi c/a)$, with width Γ

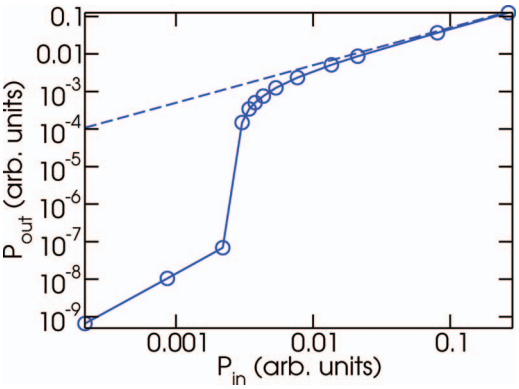

FIG. 3. (Color) Graph of power emitted at $\omega=\omega_1$ vs power absorbed at $\omega=\omega_2$ (both measures of power are in the same units). The dotted line corresponds to the maximum conversion efficiency for the values of ω_i used in this calculation. Notice a sharp rise in emission around $P_{in}\approx 0.003$, which corresponds to the lasing threshold for this system.

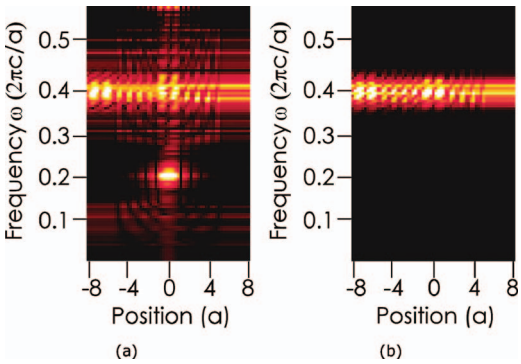

FIG. 4. (Color) Visualization of $E(x,\omega)$ in 1D Fabry-Perot cavities with active material (a) and without active material (b). The low-frequency band in the middle of (a) signifies the presence of an electronic coupling to the resonant mode in the cavity, absent in (b).

$=0.001(2\pi c/a)$, and reemit at the resonant frequency $\omega=0.2(2\pi c/a)$, with width $\Gamma=0.001(2\pi c/a)$. This traps light, thus encouraging stimulated emission. Also, the parameter values $\sigma_2=0.0008$ and $I_2=2.77$ (at the edge of the material

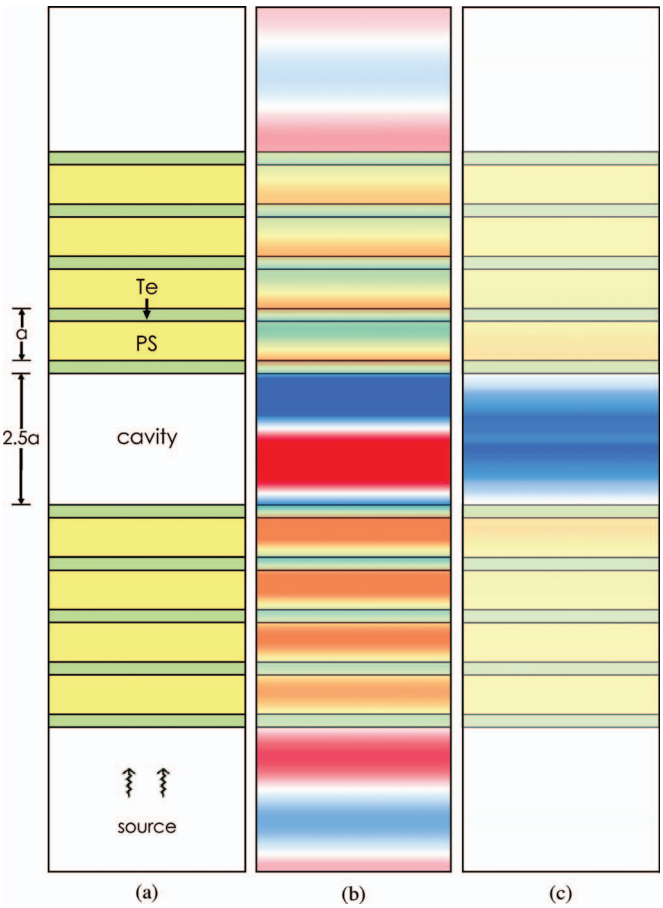

FIG. 5. (Color) Conversion of light from the optical pumping frequency ($\omega=0.4$) to the stimulated emission frequency ($\omega=0.2$ in a Fabry-Perot cavity). The geometry is illustrated in (a) with green representing high-dielectric tellurium and yellow representing lower-dielectric polystyrene. The pump pulse is shown in (b), and the stimulated emission is shown in (c), with positive electric fields corresponding to blue and negative to red.

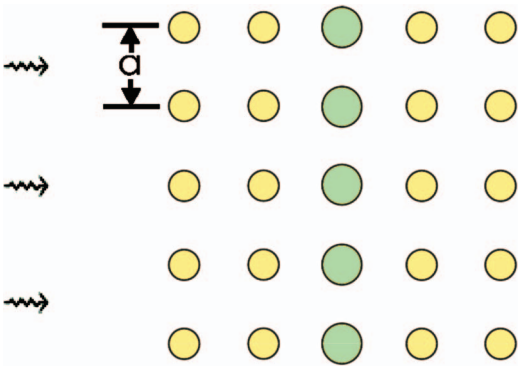

FIG. 6. (Color) Square lattice of dielectric columns, with $r=0.2a$ and $\epsilon=8.9$. A row of defect columns in the middle have $r=0.25a$, $\epsilon=17.1$.

near the source) lead to a population transfer of about 69%; furthermore, $\sigma_1=0.001$, which is large enough to create sustainable radiative transfer, and τ_{21} is set to an extremely large time, which makes nonradiative decay negligible ($\Gamma_e=\Gamma_1$) and leads to an extremely high conversion efficiency $\eta=0.9986$. Evidence for this process is given by Fig. 4 which shows intensity as a function of position and frequency. The upper band, centered around $\omega=0.4(2\pi c/a)$, corresponds to the optical pump frequency, which clearly is transmitted through the dielectric structure with relatively low reflection. The lower band, centered around $\omega=0.2(2\pi c/a)$, which only exists in the middle of the active cavity, represents the electronic coupling to the fundamental mode of the cavity. In the absence of this electronic coupling, no such band occurs, as shown on the right-hand side of Fig. 4. In general, multimode lasing could occur in an active material, but all of the calculations in this paper are designed to have nondegenerate resonant modes with a mode spacing significantly greater than the width of the population-inverted atomic transition. The field patterns associated with optical pumping and stimulated emission are shown in Fig. 5.

D. Dielectric rods in a 2D lattice

The next simulation is of a 2D system, a square lattice of dielectric rods possessing a line of defect rods. The parameters used were based on those of Ref. 24, with $\epsilon=8.9$ and $r=0.2a$ for the normal rods and $\epsilon=17.1$ and $r=0.25a$ for the defect rods. The purely dielectric system, illustrated in Fig. 6, was tested and was shown to yield a transmission peak about a frequency of $\omega=0.346(2\pi c/a)$, as shown in Fig. 7. The introduction of active material in the dielectric rods having an absorption frequency $\omega=0.5(2\pi c/a)$ and width $\Gamma=0.01(2\pi c/a)$, along with an emission frequency $\omega=0.346(2\pi c/a)$ and width $\Gamma=0.0006(2\pi c/a)$, changed the transmission spectrum as one would expect—the frequencies around $\omega=0.5(2\pi c/a)$ being depleted and the frequencies around the defect mode at $\omega=0.346(2\pi c/a)$ being strongly

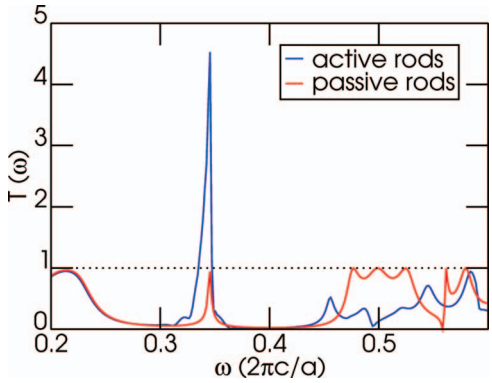

FIG. 7. (Color) Transmission for active and passive versions of the geometry shown in Fig. 6. Notice the sharp enhancement of the defect mode peak in the gap to above 100%, the signature of a gain medium.

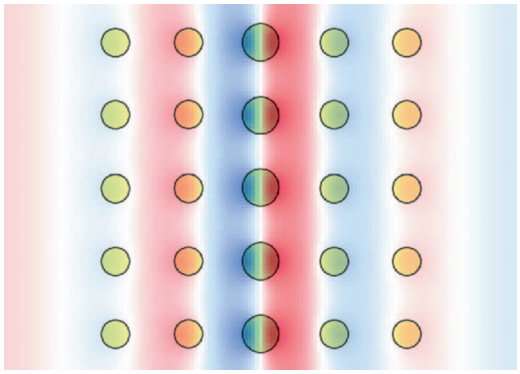

FIG. 8. (Color) Snapshot of the "π-like" defect mode centered about $\omega=0.346(2\pi c/a)$.

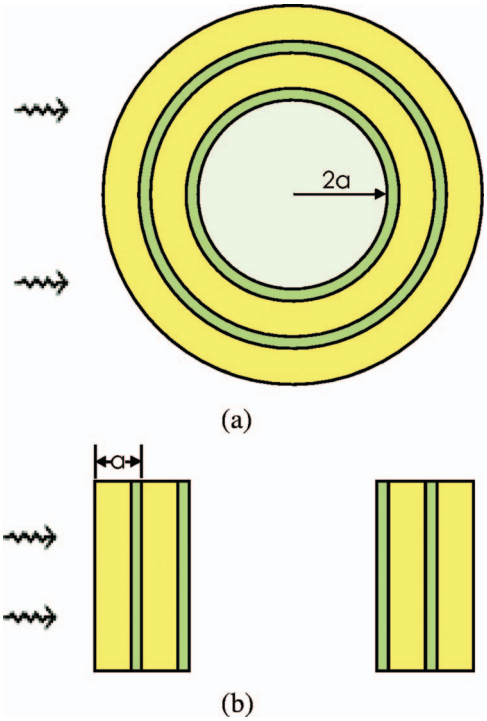

FIG. 9. (Color) Two slices of a cylindrical photonic crystal, a multilayer dielectric structure with continuous symmetry along z. Here, a core of radius $2a$ is surrounded by two bilayers of dielectric, with $\epsilon_{low}=2.56$ and $\epsilon_{high}=23.04$. (a) depicts a cross section perpendicular to the z axis, and (b) shows a cross section through the center of the core along the z axis.

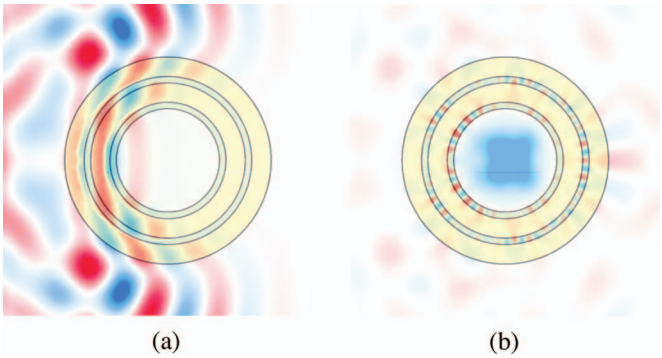

FIG. 10. (Color) Conversion of light at an optical pump frequency into a stimulated emission frequency via the TM_{01} resonant mode of a cylindrical photonic crystal with two bilayers, viewed perpendicular to the z axis. The incoming wave in (a) has $\omega \approx 0.4(2\pi c/a)$, and the outgoing wave in (b) has $\omega \approx 0.19(2\pi c/a)$.

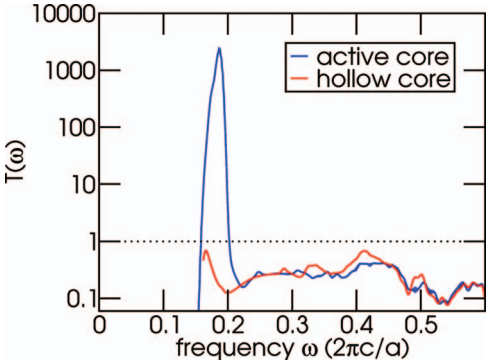

FIG. 12. (Color) Transmission for a cylindrical photonic crystal structure with and without active material at the core. Notice the slight decrease in transmission at $\omega \approx 0.4(2\pi c/a)$ and the sharp increase in transmission about $\omega \approx 0.186(2\pi c/a)$ for the active material.

enhanced. In fact, the transmission percentage for the defect mode goes above 100%, the signature of a gain medium. The comparison between the two cases is shown in Fig. 7. The parameter values $\sigma_2=0.2$ and $I_2=0.01979$ (on the right edge of the central defect rod) lead to a population transfer of about 40%; also, $\sigma_1=0.2$, which is large enough to create sustainable radiative transfer, and τ_{21} is set to an extremely large time, which makes nonradiative decay negligible ($\Gamma_e = \Gamma_1$). As a result, the efficiency of the conversion is given by $\eta=0.986$ for the parameter values used. An illustration of the defect mode is given in Fig. 8. The main defect mode, centered about $\omega=0.346(2\pi c/a)$, evidently has one nodal line, said to be "π-like."[24] Interestingly enough, one might expect this mode to couple poorly to the atoms on the defect rods due to the nodal plane, but a substantial transmission enhancement of over 300% is observed.

E. Cylindrical photonic crystal in 3D

The third simulation is of a cylindrical photonic crystal, a multilayer dielectric structure that is rolled into a cylinder, with a cross section such as the one in Fig. 9. In this paper, an external plane-wave source on the left side of the structure is used to excite an atomic material inside the otherwise hollow core. The targeted mode is the so-called TM_{01} mode, which has a nonzero E_z and H_ϕ. Further properties of the modes of cylindrical photonic crystals are discussed in Ref. 25.

Another direct illustration of optically pumped lasing is shown in Figs. 10 and 11. Here, a cylindrical photonic crystal with two bilayers of tellurium and polystyrene and an inner radius $r_i=2a$ is pumped with a broad Gaussian source centered around $\omega=0.4(2\pi c/a)$. The short cylinder of active material in the center absorbs the incoming radiation with $\omega=0.4(2\pi c/a)$ and $\Gamma=0.002(2\pi c/a)$, then re-emits near the predicted TM_{01} cutoff frequency $\omega=0.1914(2\pi c/a)$ (for $r_i = 2a$), with width $\Gamma=0.0004(2\pi c/a)$.

That this conversion takes place can be checked visually: it is evident from the before and after snapshots in Fig. 11 that the wave number decreases substantially in the horizon-

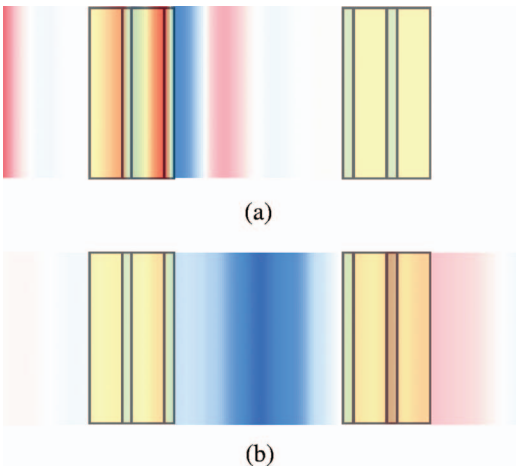

FIG. 11. (Color) Conversion of light at an optical pump frequency into a stimulated emission frequency, as in Fig. 10, but in a cross section through the center of the core along the z axis.

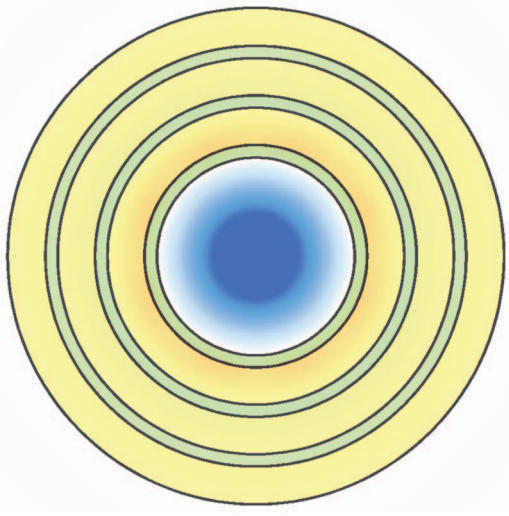

FIG. 13. (Color) Snapshot of the TM_{01} mode which is excited by a small cluster of atoms at the center of the cylindrical photonic crystal.

tal direction. Combining that observation with the rest of the information about this mode implies that the latter snapshot corresponds to a much-lower-frequency mode.

This expectation can also be checked numerically. In Fig. 12, transmission through the photonic crystal is shown for two cases: one with active material and one without. Clearly an enormous enhancement of the transmission, orders of magnitude above 100%, occurs with the introduction of the active material. This can only be due to optical pumping. A smaller but still noticeable drop in the transmission of some of the energy near $\omega=0.4(2\pi c/a)$ lends support to this conclusion. The peak in transmission occurs at $\omega=0.188(2\pi c/a)$, fairly close to our expectation of a peak at $\omega=0.1914(2\pi c/a)$. The shift in the resonant frequency in the presence of the active material can be attributed to the so-called pulling effect. The real part of the gain polarization corresponds to a small shift in the dielectric constant, which in turn shifts the resonance. The strength of the pulling effect is thus proportional to the coefficient converting electric field into polarization, which is on the order of $\xi=\sigma_i/(\omega_i\Gamma_i)$. The reason that the pulling effect was not observed previously is that $\xi=5$ in the 1D case and $\xi=964$ in the 2D case, in both cases giving rise to shifts which fall below the frequency spacing. However, $\xi=6531$ in this 3D calculation, giving rise to a substantially larger shift which in turn gives rise to fairly off-resonance coupling, broadening the emission substantially beyond the natural width and lowering the efficiency. The parameter values $\sigma_2=0.05$ and $I_2=0.0117$ (on the right side of the inner cavity, $r=1.25a$) lead to a population transfer of about 36%; also, $\sigma_1=0.5$, which is large enough to create sustainable radiative transfer, and τ_{21} is set to an extremely large time, which makes nonradiative decay negligible ($\Gamma_e=\Gamma_1$). In the end, the efficiency of this conversion process is $\eta=0.828$. Tuning the emission frequencies to the shifted values and adjusting the widths accordingly would allow the efficiency to approach the theoretical maximum. Furthermore, note that the shift in the effective index of the core material may alter the Fabry-Perot resonances and thus shift the position of the transmission peaks observed in Fig. 12. However, it is also possible that numerical errors that occur during the propagation of the fields by the atomic code may have given rise to some of the differences between the active and passive core transmission spectra, especially away from the resonant frequencies of $\omega_1=0.1914(2\pi c/a)$ and $\omega_2=0.4(2\pi c/a)$. This points to the possibility that a prediction-correction approach to the field propagation, as discussed, e.g., in Refs. 11 and 26, may be warranted for regimes of stronger polarizabilities ξ.

Finally, consider the case of a small cluster of atoms placed at the exact center of the cylindrical photonic crystal. The cluster radius is taken to be much smaller than an optical wavelength, so the atomic system can be modeled as a single point in space on the scale of the simulation. This system is studied by comparing the calculation for an empty cylindrical core to one which has an atomic cluster inside. In this calculation, the excitation frequency is $\omega=0.2857(2\pi c/a)$, with width $\Gamma=0.01(2\pi c/a)$; the emission frequency is $\omega=0.1939(2\pi c/a)$, with width $\Gamma=0.0002(2\pi c/a)$. The cluster is optically pumped by an extremely broad Gaussian source with central frequency $\omega=0.264(2\pi c/a)$. This arrangement allows for depopulation of the ground state of the central cluster followed by emission into a TM_{01} mode of nonnegligible magnitude. The differential field profile after excitation followed by stimulated emission is shown in Fig. 13. As expected, the TM_{01} mode is the one observed. The conversion efficiency of this process was found to be extremely high ($\eta>0.999$). This suggests that the scheme for biological sensing proposed in Ref. 27 would be capable of detecting very small numbers of atoms. If one were to move the cluster away from the center, coupling to the same mode would still be expected (except at the nodes). The final amplitude of the fluorescent mode for atomic clusters on or off center should be the same in the absence of other processes besides stimulated emission (neglecting modal decay). However, the threshold may be increased due to the decrease in the local density of states (which goes as the zeroth order Bessel function squared for this problem).

IV. CONCLUSION

An extension to the well-established FDTD method for simulating Maxwell's equations in macroscopic dielectric media has been developed to include active materials modeled by four-level atoms. The code was verified to display the saturation and threshold effects expected for atomic materials, in agreement with analytical results. This method is used to simulate optically pumped lasers in one, two, and three dimensions, as well as a proposed biological sensor. It is found that the key criteria for efficient conversion of energy are the delivery of the right amount of field energy to create a population inversion of order unity, as predicted by Eq. (7), and the presence of a small amount of energy at the resonant emission frequency, along with a low enough loss rate Γ_e and high enough coupling σ_1, such that the induced population inversion $|\Delta N_1(0)|>\omega_1\Gamma_e/4\pi\sigma_1$. One additional measure that can increase efficiency is concentrating atomic emitters in the regions of the defect that should have the highest field intensity in the defect mode. Simulations of the cylindrical photonic crystal system support this assertion, which is why the radius of the active material was only $1.4a$ in a cylindrical photonic crystal with $r_i=2a$ and the active material only filled the middle half of the cavity (length $1.25a$) in a 1D Fabry-Perot étalon defect cavity of size $2.5a$. Finally, a careful choice of coupling strengths and linewidths is critical for efficient conversion; any real-world system would have fixed values of these parameters which could put an important limitation on the conversion efficiency. These simulations should facilitate the design of ultralow-threshold lasers and single-fluorescent-molecule detectors. Future work should incorporate changes in the rate of spontaneous emission associated with the presence of a cavity and allow for accurate calculations of the lasing threshold.

ACKNOWLEDGMENTS

The authors would like to thank Xunya Jiang, Marin Soljacic, and David Chan for sharing their code and expertise. This work was supported in part by the Materials Research

Science and Engineering Center program of the National Science Foundation under Grant No. DMR 02-13282, the Army Research Office through the Institute for Soldier Nanotechnologies under Contract No. DAAD-19-02-D0002, and the U.S. Department of Energy under Award No. DE-FG02-99ER45778.

[1] E. Hecht, *Optics* (Addison-Wesley, Reading, MA, 1998).
[2] N. W. Ashcroft and N. D. Mermin, *Solid State Physics* (Holt Saunders, Philadelphia, 1976).
[3] G. D. Mahan, *Many-Particle Physics* (Kluwer Academic, New York, 2000).
[4] A. E. Siegman, *Lasers* (University Science Books, Sausalito, CA, 1986).
[5] C. Kittel, *Introduction to Solid State Physics* (John Wiley and Sons, New York, 1986).
[6] A. L. Schawlow and C. H. Townes, Phys. Rev. **112**, 1940 (1958).
[7] B. Toland, B. Houshmand, and T. Itoh, IEEE Microw. Guid. Wave Lett. **3**, 333 (1993).
[8] H. Cao, J. Y. Xu, D. Z. Zhang, S.-H. Chang, S. T. Ho, E. W. Seelig, X. Liu, and R. P. H. Chang, Phys. Rev. Lett. **84**, 5584 (2000).
[9] O. Painter, R. K. Lee, A. Scherer, A. Yariv, J. D. O'Brien, P. D. Dapkus, and I. Kim, Science **284**, 1819 (1999).
[10] J. Vučković, O. Painter, Y. Xu, A. Yariv, and A. Scherer, IEEE Trans. Magn. **35**, 1168 (1999).
[11] R. W. Ziolkowski, J. M. Arnold, and D. M. Gogny, Phys. Rev. A **52**, 3082 (1995).
[12] A. S. Nagra and R. A. York, IEEE Trans. Antennas Propag. **46**, 334 (1998).
[13] R. W. Ziolkowski, IEEE Trans. Antennas Propag. **45**, 375 (1997).
[14] G. Slavcheva, J. M. Arnold, I. Wallace, and R. W. Ziolkowski, Phys. Rev. A **66**, 063418 (2002).
[15] S. John and G. Pang, Phys. Rev. A **54**, 3642 (1996).
[16] X. Jiang and C. M. Soukoulis, Phys. Rev. Lett. **85**, 70 (2000).
[17] C. M. Soukoulis, X. Jiang, J. Y. Xu, and H. Cao, Phys. Rev. B **65**, 041103(R) (2002).
[18] C. Vanneste and P. Sebbah, Phys. Rev. Lett. **87**, 183903 (2001).
[19] P. Sebbah and C. Vanneste, Phys. Rev. B **66**, 144202 (2002).
[20] H. Cao, J. Phys. A **38**, 10497 (2005).
[21] T. Harayama, S. Sunada, and K. S. Ikeda, Phys. Rev. A **72**, 013803 (2005).
[22] S.-H. Chang and A. Taflove, Opt. Express **12**, 3827 (2004).
[23] K. S. Yee, IEEE Trans. Antennas Propag. **14**, 302 (1966).
[24] J. D. Joannopoulos, R. D. Meade, and J. N. Winn, *Photonic Crystals: Molding the Flow of Light* (Princeton University Press, Princeton, 1995).
[25] S. G. Johnson, M. Ibanescu, M. A. Skorobogatiy, O. Weisberg, T. Engeness, M. Soljacic, S. A. Jacobs, J. D. Joannopoulos, and Y. Fink, Opt. Express **9**, 748 (2001).
[26] F. Schlottau, M. Piket-May, and K. Wagner, Opt. Express **13**, 182 (2005).
[27] P. Bermel, J. D. Joannopoulos, Y. Fink, P. A. Lane, and C. Tapalian, Phys. Rev. B **69**, 035316 (2004).